

# MimiCAT: Mimic with Correspondence-Aware Cascade-Transformer for Category-Free 3D Pose Transfer

Zenghao Chai<sup>1</sup> Chen Tang<sup>2</sup> Yongkang Wong<sup>1</sup> Xulei Yang<sup>3</sup> Mohan Kankanhalli<sup>1</sup>

<sup>1</sup>School of Computing, National University of Singapore

<sup>2</sup>MMLab, The Chinese University of Hong Kong <sup>3</sup>Institute for Infocomm Research, A\*STAR

zenghaochai@gmail.com mohan@comp.nus.edu.sg

DOI <https://doi.org/10.48550/arXiv.2511.18370>

URL <https://MimiCAT.github.io>

## Abstract

3D pose transfer aims to transfer the pose-style of a source mesh to a target character while preserving both the target’s geometry and the source’s pose characteristic. Existing methods are largely restricted to characters with similar structures and fail to generalize to **category-free** settings (e.g., transferring a humanoid’s pose to a quadruped). The key challenge lies in the structural and transformation diversity inherent in distinct character types, which often leads to mismatched regions and poor transfer quality. To address these issues, we first construct a million-scale pose dataset across hundreds of distinct characters. We further propose MimiCAT, a cascade-transformer model designed for category-free 3D pose transfer. Instead of relying on strict one-to-one correspondence mappings, MimiCAT leverages semantic keypoint labels to learn a novel soft correspondence that enables flexible many-to-many matching across characters. The pose transfer is then formulated as a conditional generation process, in which the source transformations are first projected onto the target through soft correspondence matching and subsequently refined using shape-conditioned representations. Extensive qualitative and quantitative experiments demonstrate that MimiCAT transfers plausible poses across different characters, significantly outperforming prior methods that are limited to narrow category transfer (e.g., humanoid-to-humanoid).

## 1. Introduction

Recent advancements in computer graphics and vision have led to remarkable progress in modeling articulated 3D characters [27, 48, 53, 73, 75]. Among their key properties, articulated poses play a crucial role in conveying the behaviors and emotions of diverse types of characters. Once poses and animations are created, reusing them for novel characters and scenarios—a.k.a. 3D pose transfer [3, 42, 60, 71]—

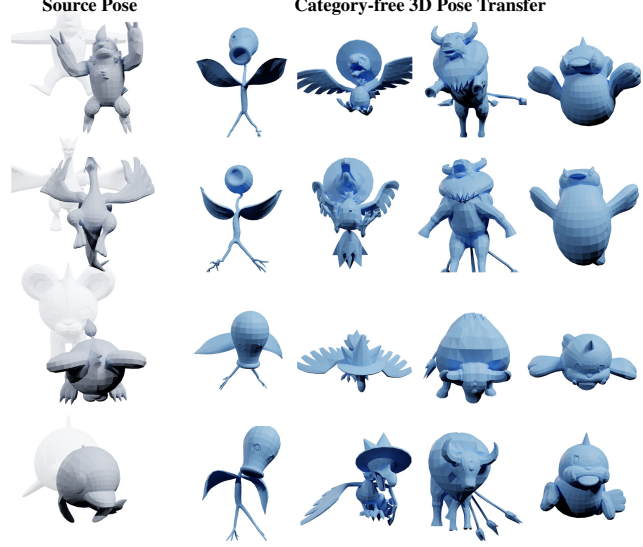


Figure 1. **MimiCAT for category-free 3D pose transfer.** Given source character with desired poses (left), our model faithfully transfers the given pose to the target characters (right) across completely different categories, proportions and topologies, without requirement of manually labeled correspondence.

becomes highly desirable. The objective is to apply a reference pose from a source character to a target character while simultaneously preserving the unique characteristics of the target and the fidelity of the source pose. However, transferring poses across different characters is highly non-trivial. Compared to humanoids, many characters possess distinct body structures and proportions, making reproducing similar behaviors challenging. The task is often dependent on experienced 3D artists, making it both expensive and slow.

While early works [8, 9, 60, 61] have shown promising results for pose transfer between characters with similar morphology (e.g., from a human to a robot) by learning keypoint- or vertex-level correspondences, they struggle to generalize across arbitrary character categories (e.g., transferring bird poses to humanoids). A key limitation is their

Table 1. **Statistics of character motion datasets.** Our dataset is compared against representative publicly available motion datasets in terms of rigging, number of characters, and motion coverage.

Dataset	Rigging	#Characters	#Motions	#By Artist
Mixamo [1]	✓	118	2,000	✓
AMASS [37]	✓	346	11,451	✓
TruebonesZoo [58]	✓	70	1,000	✓
PlanetZoo [65]	✓	251	251	✗
DT4D-A [30]	✗	71	1,772	✓
PokeAnimDB (Ours)	✓	975	28,809	✓

reliance on one-to-one mappings to establish correspondences. Such mappings are often inadequate for modeling complex many-to-many relationships—for example, shall four limbs of a humanoid correspond to the two wings of a bird? This mismatch leads to significant transfer artifacts when dealing with characters of fundamentally different topologies. Moreover, existing approaches typically learn pose priors from human motion datasets [1, 21, 37, 64], making them prone to out-of-distribution failures (*e.g.*, unnatural artifacts). For instance, transferring human poses to birds can yield degraded results due to the lack of knowledge about bird-specific motion patterns. These challenges arise because different characters exhibit highly diverse and complex structures (*e.g.*, keypoints, skinning weights, and topologies), and their keypoints exhibit distinct rotation patterns conditioned on each character’s morphology and rigging design. These factors collectively make cross-category 3D pose transfer a highly challenging problem.

To address the above challenges, we first construct a large-scale pose dataset containing  $\sim 4.4$  million pose samples across hundreds of diverse character categories (see Tab. 1). Using this dataset, we pretrain a shape-aware distribution model that captures the joint distribution of keypoint-wise rotations [40, 50, 70] for characters with varying skeletal structures. This pretrained distribution model serves as a regularization for pose transfer and prevents degenerate transformations. Following this, we introduce MimiCAT, a transformer-based [59] framework for category-free 3D pose transfer. MimiCAT features two cascaded transformer modules, which undergo two-stage training. In the first stage, a *correspondence transformer* learns a similarity matrix between two sets of keypoints with varying lengths. Rather than relying on rigid one-to-one mappings, we incorporate semantic skeleton labels (*i.e.*, keypoint names) to establish flexible many-to-many soft correspondences between structurally distinct characters. In the second stage, the estimated soft correspondences map initial transformations from the source to the target. Conditioned on pretrained shape encoders [81], we formulate pose transfer as a conditional generation problem and employ a *pose transfer transformer* to generate realistic target poses. This stage employs a self-supervised cycle-consistency loss, eliminating the need for paired cross-category ground-truth.

To evaluate the transfer quality for category-free pose transfer, we establish a new benchmark based on cross-transfer cycle consistency. In addition, following previous works [31, 60, 61], we also include humanoid-to-humanoid evaluations for comprehensive comparisons. We conduct both qualitative and quantitative experiments to demonstrate that MimiCAT can effectively transfer poses across 3D characters with significantly different morphologies, outperforming existing methods that are restricted to structural-similar characters. Once trained, our model seamlessly supports several downstream tasks, such as text-to-any-character motion generation.

In summary, our main contributions are as follows:

1. We extend the 3D pose transfer task to a broader and more challenging setting, namely *category-free pose transfer*, and construct a novel benchmark based on cycle-consistency evaluation to assess transfer quality.
2. We build a large-scale dataset containing millions of character poses across diverse categories, which enables learning 3D pose transfer models under more practical and generalizable conditions.
3. We design a novel cascade-transformer architecture, MimiCAT, that learns many-to-many soft correspondences between keypoints, enabling effective 3D pose transfer across characters with distinct structures.
4. We achieve state-of-the-art pose transfer quality and demonstrate the strong potential of our framework for downstream applications. Code and dataset will be made publicly available for research purposes.

## 2. Related Work

**Automatic 3D Object Rigging.** 3D Rigging, the task of predicting skeletons and skin weights for a 3D mesh, is a fundamental problem in computer graphics [41, 57, 68, 76, 78]. Driven by the accessibility of open-source datasets, learning-based methods have outperformed traditional manual rigging. However, most public datasets either focus on static meshes [16, 54, 67, 68], or provide animations restricted to narrow categories such as humanoids [1, 33, 35] or quadrupeds [30, 65]. Building upon these datasets, automatic rigging methods [16, 32, 41, 45, 54, 68] aim to predict skeletons and skin weights directly from geometry. To enable animating previously static characters through predicted skeletons, such methods often remain dependent on handcrafted correspondences or manually curated motions.

**Correspondence learning** constitutes a fundamental challenge in vision and graphics [17, 62, 63, 66, 79], and is particularly crucial for pose transfer. However, establishing reliable mappings between non-rigid meshes remains highly challenging. Dense correspondence methods [36, 44, 52] predict per-vertex mappings by optimizing complex energies, but are computationally expensive,

unstable, and generalize poorly beyond limited categories. Recent works [2, 12, 31, 39, 42, 71] instead consider sparse correspondences at the vertex or keypoint level, often using self-supervised learning to avoid the need for ground-truth dense annotations. These approaches are more flexible and can leverage existing rigging datasets [30, 68], but typically assume one-to-one mappings and remain restricted to intra-categories, struggling to handle cross-category correspondences (*e.g.*, between humanoids and quadrupeds).

In contrast, we construct a dataset spanning diverse categories and character-level animations, and leverage semantic keypoint annotations to supervise many-to-many soft correspondences. This allows correspondence learning across characters with length-variant keypoints, providing a stronger foundation for cross-category pose transfer.

**3D Pose Transfer.** Deformation transfer, *i.e.*, the process of retargeting and transferring 3D poses across characters, is essential for animation, simulation, and virtual content creation. [7, 22, 28, 53, 64, 69, 72, 80]. Early works [4, 5, 20, 56] formulate deformation transfer as an optimization problem, but require handcrafted correspondences (*e.g.*, point- or pose-wise) that are costly and non-scalable. Recent motion transfer methods [13, 29] suffer from a reliance on exemplar motions from the target character, which constraints their applicability when such data is unavailable. Skeleton- or handle-based models [12, 31] predict relative transformations between keypoints, but typically assume one-to-one correspondences and are trained on pose datasets with limited human characters [1, 30, 37]. As a result, they struggle to generalize across categories with inherently different skeletal structures. To bypass explicit correspondence supervision, recent works adopt implicit deformation fields [3], adversarial learning [8, 11], cycle-consistency training [18, 82], or conditional normalization layers [10, 60]. Nevertheless, these methods remain restricted to structurally similar characters and fail on stylized or cross-species transfers.

Recent novel large-scale articulation datasets [15, 16, 54] have enabled learning high-quality geometric features and reliable skeleton predictions [54] across diverse species. Drawing on these insights, we leverage pretrained shape encoders alongside a novel dataset of diverse animations to propose a cascade-transformer framework that extends pose transfer beyond humanoids to a broad range of characters.

### 3. Methodology

#### 3.1. Preliminary

**Task Definition.** Given a source character in canonical pose  $\bar{\mathbf{V}}^{\text{src}} \in \mathbb{R}^{N^{\text{src}} \times 3}$ , its posed instance  $\mathbf{V}^{\text{src}}$  with pose parameters  $\mathbf{p}$ , and a target character in canonical pose  $\bar{\mathbf{V}}^{\text{tgt}} \in \mathbb{R}^{N^{\text{tgt}} \times 3}$ , the objective of pose transfer is to generate

the posed target mesh  $\hat{\mathbf{V}}^{\text{tgt}}$ . Formally, we seek a mapping  $f(\mathbf{V}^{\text{src}}, \bar{\mathbf{V}}^{\text{src}}, \bar{\mathbf{V}}^{\text{tgt}}) \rightarrow \hat{\mathbf{V}}^{\text{tgt}}$ , where  $\hat{\mathbf{V}}^{\text{tgt}}$  retains the target’s geometry while transferring the pose  $\mathbf{p}$  from the source.

**Character Articulation Formulation.** We follow [12, 31] to represent character deformations via keypoints and skin weights. The keypoints  $\mathbf{C} \in \mathbb{R}^{K \times 3}$  together with per-vertex skin weights  $\mathbf{W} \in \mathbb{R}^{N \times K}$  are estimated by pretrained model [68]. The number of keypoints  $K$  may vary across characters (denoted as  $K_1$  and  $K_2$  for source and target characters). The deformation of a character is achieved by assigning per-keypoint transformation  $\mathbf{T} \in \mathbb{R}^{K \times 7}$ , and applying linear blend skinning (LBS) [24] to deform the mesh from canonical space to posed space:

$$\mathbf{v}_i = \sum_{k=1}^K \mathbf{w}_{i,k} \mathbf{T}_k (\bar{\mathbf{v}}_i - \bar{\mathbf{c}}_k), \quad \forall \bar{\mathbf{v}}_i \in \bar{\mathbf{V}}, \quad (1)$$

where  $\bar{\mathbf{c}}_k \in \bar{\mathbf{C}}$  denotes the canonical keypoints. For the posed character, the corresponding keypoints  $\mathbf{c}_k$  are approximated by the weighted average of the deformed vertices.

**Geometry Priors.** We utilize a pretrained 3D shape encoder  $\mathcal{E}$  [81] to extract geometry features  $\mathbf{f}_{\mathcal{E}} \in \mathbb{R}^{l_{\mathcal{E}} \times d}$  from a given character mesh, where  $l_{\mathcal{E}}$  denotes the number of query tokens. We extract geometry features for the canonical source ( $\mathbf{f}_{\bar{\mathbf{V}}^{\text{src}}}$ ), posed source ( $\mathbf{f}_{\mathbf{V}^{\text{src}}}$ ), and canonical target characters ( $\mathbf{f}_{\bar{\mathbf{V}}^{\text{tgt}}}$ ). In addition, we define the residual geometry feature of the source character as  $\delta_{\mathbf{f}} = \mathbf{f}_{\mathbf{V}^{\text{src}}} - \mathbf{f}_{\bar{\mathbf{V}}^{\text{src}}}$ , which captures the deformation difference between the posed and canonical source meshes in latent space.

#### 3.2. Motivation

**Challenges.** Humans possess the cognitive flexibility to imagine how animals imitate human behaviors and vice versa. In contrast, most existing pose transfer approaches remain restricted to narrow settings (*e.g.*, humanoid-to-humanoid). A more general and practical goal is *category-free pose transfer* across diverse characters. However, it is substantially more challenging, with two key obstacles:

- 1. Diverse skeletons and geometries.** Characters differ drastically in skeletal structure, geometric topology, and mesh density. Directly estimating per-vertex correspondences across such variations is infeasible. A common workaround is to employ intermediate representations such as keypoints. Yet, existing works assume a fixed set of keypoints across categories, overlooks the inherent variation in anatomical structures (*e.g.*, bones, limbs, and wings). This mismatch makes one-to-one keypoint mapping unreliable and often degrades transfer quality.
- 2. Scarcity of paired data.** Datasets with diverse characters and artist-designed poses are extremely limited. As a result, most existing pose transfer methods rely on reference poses from large-scale humanoid datasets with only

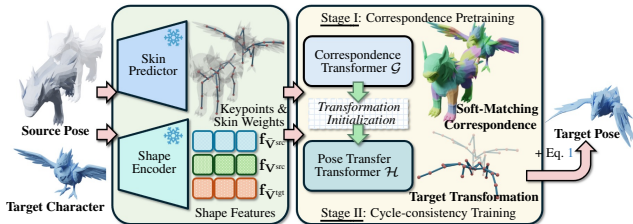


Figure 2. **Overview of MimiCAT for category-free pose transfer.** MimiCAT takes a paired source pose and target character as input. It first employs the correspondence transformer  $\mathcal{G}$  to estimate soft keypoint correspondences, then refines the initialized transformations using the pose transfer transformer  $\mathcal{H}$  to generate the target transformations. Finally, the target character is deformed into the desired pose through linear blend skinning (LBS).

a few animal samples, which prevents them from generalizing to non-human characters. Moreover, the absence of ground-truth keypoint correspondences makes it difficult for models to learn accurate mappings in a purely self-supervised manner. Creating such correspondences manually is prohibitively costly and labor-intensive.

**Overview.** To tackle these challenges, we collect a new dataset of high-quality skeletons and diverse character motions spanning humanoids, quadrupeds, birds, and more. Building on this, we introduce MimiCAT, a cascade-transformer architecture designed for category-free pose transfer. MimiCAT learns soft correspondences across keypoints of different meshes and transfers poses accordingly. An overview of our framework is illustrated in Fig. 2, and the following sections detail our technical contributions.

### 3.3. Data Collection

**Collecting Diverse Character Motions.** To overcome the above challenges and enable generalization across character categories, we curate a new dataset, PokeAnimDB, from the web consisting of high-quality, artist-designed motions for a wide range of characters. These motions span various actions, such as running, sleeping, eating, and fighting.

For efficient training, we follow prior works [16, 31, 68] to resample each character mesh into 5,000 faces and recompute skinning weights via barycentric interpolation based on the artist-provided per-vertex weights. We additionally record bone names for each character, which provide structural cues in the text domain and enable connections across categories (*e.g.*, the label “limbs” can correspond to “arms” for humanoids and “wings” for birds). All meshes are unified into *.obj* format, while skeletal animations are stored in *.bvh* format for consistency.

**Dataset Statistics.** Tab. 1 summarizes PokeAnimDB in comparison with existing publicly available animation datasets. Unlike prior collections, our dataset comprises 975 characters spanning a broad spectrum of species and



Figure 3. **Pose examples from the PokeAnimDB.** Our dataset covers a wide range of species (including humanoids, insects, quadrupeds, fishes, *etc.*) with high-quality, artist-designed poses.

morphologies, including humanoids, quadrupeds, birds, reptiles, fishes, and insects. The number of skeletal joints ranges from 11 to 241, with an average of 83. Each character is paired with artist-designed skeletal animations, resulting in a total of 28,809 motions and 4,473,481 frames, which is comparable in scale to the widely-used human motion datasets [37]. Examples that highlight the diversity and quality of our dataset are illustrated in Fig. 3.

**Pose Prior.** Based on the large-scale pose dataset, we train a transformer-based pose prior model  $\mathcal{F}$ . The model learns the distribution of plausible keypoint rotations sampled from the dataset across diverse characters, and model each rotation as a matrix-Fisher distribution [40, 50, 70]. The trained  $\mathcal{F}$  predicts per-keypoint distribution parameters  $\hat{\mathbf{F}}$  for given poses, providing a statistical prior that (1) regularizes the rotation space during pose transfer training, and (2) helps ensure the generated transformations follow realistic, physically consistent patterns across different character morphologies. Details of  $\mathcal{F}$  can be found in Appendix.

### 3.4. Cascade-Transformer for 3D Pose Transfer

To achieve category-free pose transfer, we propose a cascade-transformer model, MimiCAT, that learns soft keypoint correspondences for shape-aware deformations and is trained with a two-stage scheme.

**Shape-aware Keypoint Correspondence.** We design a *correspondence transformer*  $\mathcal{G}$  that integrates shape conditioning to estimate soft correspondences between keypoint pairs of varying lengths. Given canonical keypoints  $\bar{\mathbf{C}}^{\text{src}}$  and  $\bar{\mathbf{C}}^{\text{tgt}}$  from the source and target characters, respectively,  $\mathcal{G}$  predicts a similarity matrix  $\mathbf{S} \in \mathbb{R}^{K_1 \times K_2}$  and its normalized counterpart, a doubly-stochastic matrix  $\mathbf{M}$ , representing the probabilistic correspondence between keypoints. An overview of the  $\mathcal{G}$  architecture is shown in Fig. 4.

In contrast to GNN-based models [62, 63] that rely on skeletal connectivity priors and may not generalize well to characters with diverse hierarchical structure, we directly encode spatial coordinates of keypoints using MLP layers to obtain keypoint tokens  $\mathbf{g}_C \in \mathbb{R}^{K \times d_c}$ . To enhance discrim-

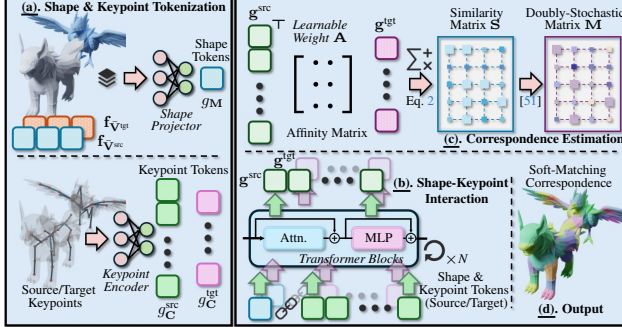


Figure 4. **Overview of the correspondence transformer  $\mathcal{G}$ .** We (a) first extract shape and keypoint tokens using the shape projector and keypoint encoder, (b) fuse shape conditions with respective keypoint latents through transformer blocks, (c) estimate correspondences via learnable affinity weights followed by the Sinkhorn algorithm, and (d) produce soft-matching correspondences between the given characters.

ination between correlated body parts, we further incorporate shape features  $\mathbf{f}_{\bar{V}^{\text{src}}}$  and  $\mathbf{f}_{\bar{V}^{\text{tgt}}}$  extracted from pretrained models [81]. These features are concatenated and processed by MLP layers to produce high-dimensional shape tokens  $\mathbf{g}_M \in \mathbb{R}^{L \times d_C}$ . The shape tokens are then combined with the keypoint tokens to form  $[\mathbf{g}_M, \mathbf{g}_C]$ , which are fed into transformer blocks to learn shape-aware latent representations  $\mathbf{g}^{\text{src}}$  and  $\mathbf{g}^{\text{tgt}}$  for the source and target keypoints.

The pairwise similarity matrix  $\mathbf{S}$  between the source and target latent features is computed using a learnable affinity matrix  $\mathbf{A}$ . The resulting similarity scores are exponentiated and normalized into a doubly stochastic correspondence matrix  $\mathbf{M}$  via the Sinkhorn algorithm [51], where each entry  $\mathbf{M}_{i,j}$  represents the soft matching probability between a source and a target keypoint:

$$\mathbf{S} = \exp \left( \mathbf{g}^{\text{src}} \top \mathbf{A} \mathbf{g}^{\text{tgt}} \right), \quad \mathbf{M} = \text{Sinkhorn}(\mathbf{S}). \quad (2)$$

**Correspondence-aware Transformation Initialization.** Given the canonical and posed meshes, keypoints, and skin weights of the source character, we first follow [6, 31] to estimate per-keypoint transformations  $\mathbf{T}^{\text{src}} = \{\mathbf{T}_1^{\text{src}}, \dots, \mathbf{T}_{K_1}^{\text{src}}\}$ , where each transformation  $\mathbf{T}_i^{\text{src}}$  includes a rotation quaternion  $\mathbf{q}_i$  and a translation vector  $\mathbf{t}_i$ .

Using the correspondence matrix  $\mathbf{M}$  from Eq. 2, the initial transformations of the target character are obtained by aggregating the source transformations according to the matching probabilities. For each target keypoint  $\mathbf{c}_j \in \mathbf{C}^{\text{tgt}}$ , its translation  $\bar{\mathbf{t}}_j$  and associated query position  $\bar{\mathbf{c}}_j$  in the source character are calculated as weighted averages:

$$\bar{\mathbf{x}}_j = \left( \sum_{i=1}^{K_1} \mathbf{M}_{i,j} \right)^{-1} \sum_{i=1}^{K_1} \mathbf{x}_i \mathbf{M}_{i,j}, \quad \mathbf{x}_i \in \{\mathbf{t}_i, \mathbf{c}_i\}. \quad (3)$$

Directly averaging quaternions, however, is invalid because it neither guarantees unit-norm rotations nor resolves

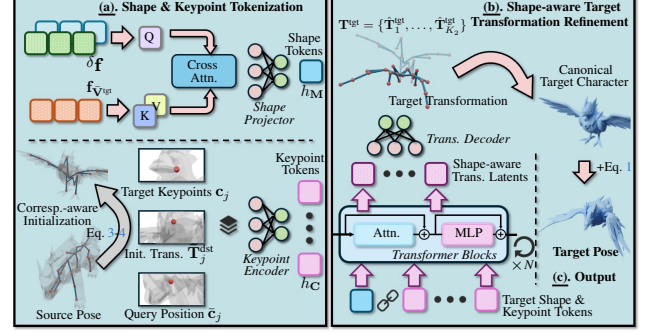


Figure 5. **Overview of the pose transfer transformer  $\mathcal{H}$ .** We (a) first perform cross-attention to extract deformation-aware cues for shape tokenization and apply correspondence-aware initialization for keypoint tokenization. (b) The shape and keypoint tokens are fed into transformer blocks to derive high-level representations, and decode into refined target transformations. (c) the posed target mesh is generated by deforming the canonical target through Eq. 1.

the inherent 2:1 ambiguity of quaternions—often leading to inconsistent or flipped orientations (see Fig. 9). Instead, we compute the weighted average rotation by minimizing the Frobenius norm between attitude matrices:

$$\bar{\mathbf{q}}_j = \arg \min_{\mathbf{q}_j \in \mathbb{S}^3} \sum_{i=1}^{K_1} \mathbf{M}_{i,j} \|\mathbf{A}(\mathbf{q}_j) - \mathbf{A}(\mathbf{q}_i)\|_F^2, \quad (4)$$

where  $\mathbf{A}(\mathbf{q}) \in \text{SO}(3)$  denotes the attitude matrix of quaternion  $\mathbf{q}$ . Following [38, 43], the solution  $\bar{\mathbf{q}}_j$  is given by the eigenvector corresponding to the largest eigenvalue of the weighted covariance matrix, *i.e.*,  $\sum_{i=1}^{K_1} \mathbf{M}_{i,j} \mathbf{q}_i \mathbf{q}_i^\top$ .

**Shape-aware Pose Transfer.** Given the initialized transformations, our goal is to refine them into the final target transformations while incorporating geometric conditions. To achieve this, we design a *pose transfer transformer*  $\mathcal{H}$  that maps shape and keypoint features to per-keypoint transformations of the target character, as illustrated in Fig. 5.

We extract geometry features  $\mathbf{f}_{\bar{V}^{\text{src}}}, \mathbf{f}_{\bar{V}^{\text{tgt}}}, \mathbf{f}_{\bar{V}^{\text{tgt}}}$  from the canonical and posed source meshes and the canonical target mesh, respectively. These features are fused through cross-attention layers to inject the residual source deformation cues  $\delta_f$  into the target representation, producing geometry-condition tokens  $\mathbf{h}_M$ . For the keypoint representation, each target keypoint  $\mathbf{c}_j$  is paired with its query position  $\bar{\mathbf{c}}_j$  and initialized transformation  $\bar{\mathbf{t}}_j, \bar{\mathbf{q}}_j$ . The concatenated vector  $[\mathbf{c}_j, \bar{\mathbf{c}}_j, \bar{\mathbf{t}}_j, \bar{\mathbf{q}}_j]$  is then projected through MLP layers to form high-dimensional keypoint tokens  $\mathbf{h}_C \in \mathbb{R}^{K_2 \times d_C}$ .

Finally, the geometry tokens  $\mathbf{h}_M$  and keypoint tokens  $\mathbf{h}_C$  are concatenated to form  $[\mathbf{h}_M, \mathbf{h}_C]$  and fed into transformer blocks, producing shape-aware latent features. MLP layers decode these features into per-keypoint transformations  $\mathbf{T}^{\text{tgt}} = \{\hat{\mathbf{T}}_1^{\text{tgt}}, \dots, \hat{\mathbf{T}}_{K_2}^{\text{tgt}}\}$ , which are applied to deform the canonical target mesh into final posed mesh  $\hat{\mathbf{V}}^{\text{tgt}}$  via Eq. 1.

### 3.5. Training, Inference & Objective Functions

**Text-Guided Ground-truth Correspondence.** A key prerequisite for correspondence learning is access to reliable “ground-truth” matches. However, manually annotating either keypoint- or vertex-level correspondences for large-scale pairs is highly non-trivial and labor-intensive.

Fortunately, the artist-designed characters themselves furnish semantic keypoint names. For example, the arms of humanoids and the wings of birds are both labeled as “limbs”, which aligns with human perception of their functional similarity. Drawing from this observation, we bypass handcrafting correspondences or designing sophisticated algorithms [66, 74]. Instead, we use CLIP  $\mathcal{E}_{\text{CLIP}}$  [49] to encode the textual labels of keypoints  $\mathbf{c}_k$  into latent space, yielding  $\mathbf{f}_k$ . We compute the similarity matrix  $\mathbf{S}_{\text{cos}} \in \mathbb{R}^{K_1 \times K_2}$  via cosine similarity, each element  $s_{i,j}$  given by:

$$s_{i,j} = \frac{\mathbf{f}_i \cdot \mathbf{f}_j}{\|\mathbf{f}_i\| \|\mathbf{f}_j\|}, \quad (5)$$

where  $s_{i,j}$  measures the similarity between source and target characters  $\mathbf{c}_i \in \mathbf{C}^{\text{src}}$  and  $\mathbf{c}_j \in \mathbf{C}^{\text{tgt}}$ . Finally, we normalize  $\mathbf{S}_{\text{cos}}$  using the Hungarian algorithm [26] to obtain ground-truth one-hot correspondence  $\mathbf{M}_{\text{hung}}$ . Fig. 6 showcase examples of our text-based ground-truth *v.s.* hierarchical correspondence [74].

**Two-Stage Training.** We train MimiCAT using two-stage process. In the first stage, we train the correspondence transformer  $\mathcal{G}$ . We note that multiple keypoints from the source character may correspond to a single keypoint in the target, and vice versa. Therefore, in addition to the hard one-to-one mapping  $\mathbf{M}_{\text{hung}}$  obtained via the Hungarian algorithm, we introduce a soft-matching matrix  $\mathbf{M}_{\text{sink}} = \text{Sinkhorn}(\mathbf{S}_{\text{cos}})$ , which captures many-to-many correlations between source and target keypoints. We then use the Frobenius norm to jointly encourage the predicted affinity matrix  $\mathbf{S}$  to align with the text-based cosine similarity matrix  $\mathbf{S}_{\text{cos}}$ , while maintaining consistency between the predicted correspondence  $\mathbf{M}$ , the soft Sinkhorn mapping  $\mathbf{M}_{\text{sink}}$ , and the hard assignment  $\mathbf{M}_{\text{hung}}$ :

$$\mathcal{L}_{\text{forb}} = \|\mathbf{S} - \mathbf{S}_{\text{cos}}\|_2^2 + \|\mathbf{M} - \mathbf{M}_{\text{sink}}\|_2^2 + \|\mathbf{M} - \mathbf{M}_{\text{hung}}\|_2^2. \quad (6)$$

In the second stage, we freeze the correspondence transformer  $\mathcal{G}$  and train the pose transfer transformer  $\mathcal{H}$  using a cycle-consistency objective. Since ground-truth targets are unavailable for cross-category pairs, we adopt a self-supervised strategy that reconstructs the source character from its transferred pose. Specifically, we first transfer the pose from the source to the target, and then back from the predicted target to the source. The reconstruction loss encourages the recovered source mesh to match the given one:

$$\mathcal{L}_{\text{rec}} = \|\hat{\mathbf{V}}^{\text{src}} - \mathbf{V}^{\text{src}}\|_2^2, \quad (7)$$

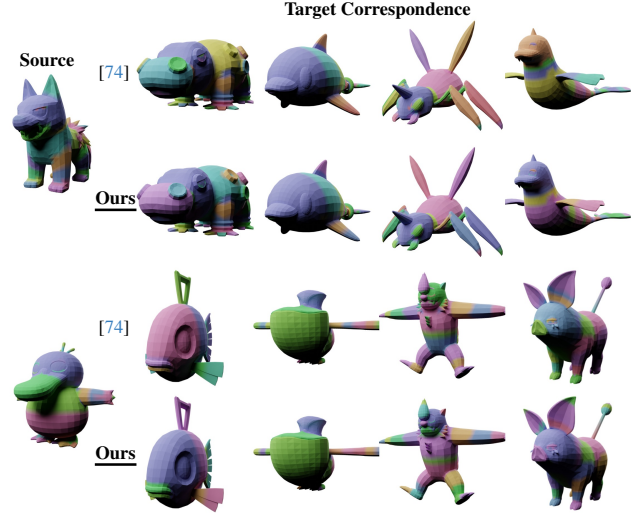


Figure 6. **Correspondence visualization.** We visualize correspondences from source characters (*left*) to category-free targets (*right*). Compared with the hierarchical correspondence algorithm [66, 74], our text-guided correspondence yields more coherent and semantically consistent part alignments across characters.

where  $\hat{\mathbf{V}}^{\text{tgt}} = f(\mathbf{V}^{\text{src}}, \bar{\mathbf{V}}^{\text{src}}, \bar{\mathbf{V}}^{\text{tgt}})$  and  $\hat{\mathbf{V}}^{\text{src}} = f(\hat{\mathbf{V}}^{\text{tgt}}, \bar{\mathbf{V}}^{\text{tgt}}, \bar{\mathbf{V}}^{\text{src}})$ .

To further regularize rotations, we employ the pretrained pose prior model  $\mathcal{F}$ . Given the ground-truth posed character  $\mathbf{V}^{\text{src}}$ , we use  $\mathcal{F}$  to estimate the pose distribution parameters  $\hat{\mathbf{F}}$  of each keypoints. Then, if the predicted rotation  $\hat{\mathbf{q}}_k$  for  $k$ -th keypoint is reasonable, we assume it shows the max log-likelihood given the distribution parameters based on  $\mathbf{V}^{\text{src}}$ . Hence, we enforce the estimated rotation to preserve minimal negative log-likelihood (NLL) properties [40, 50].

$$\begin{aligned} \mathcal{L}_{\text{reg}} &= - \sum_{k=1}^K \log p(A(\hat{\mathbf{q}}_k) | \hat{\mathbf{F}}_k) \\ &= \sum_{k=1}^K \left( \log c(\hat{\mathbf{F}}_k) - \text{tr}(\hat{\mathbf{F}}_k^\top A(\hat{\mathbf{q}}_k)) \right), \end{aligned} \quad (8)$$

where  $\hat{\mathbf{F}}_k$  denotes the predicted distribution parameters for the  $k$ -th keypoint,  $c(\hat{\mathbf{F}}_k)$  is the normalization constant w.r.t. the distribution parameters  $\hat{\mathbf{F}}_k$ .

Additionally, we encourage the reconstructed meshes in the cycle process to preserve consistent high-level geometric features with their original posed counterparts by enforcing feature-space consistency,  $\mathcal{L}_{\text{feat}} = \|\mathcal{E}(\hat{\mathbf{V}}^{\text{src}}) - \mathcal{E}(\mathbf{V}^{\text{src}})\|_2^2$ .

**Inference Stage.** During inference, given the canonical poses of both the source and target characters, we first apply the pretrained skeleton prediction model [68] to obtain their corresponding skin weights and skeleton structures. MimiCAT then deforms the source pose into the target character according to the learned soft correspondences and transformation mappings. Finally, following prior works [31, 77], we perform test-time refinement using an as-rigid-as-possible (ARAP) [55] optimization to en-

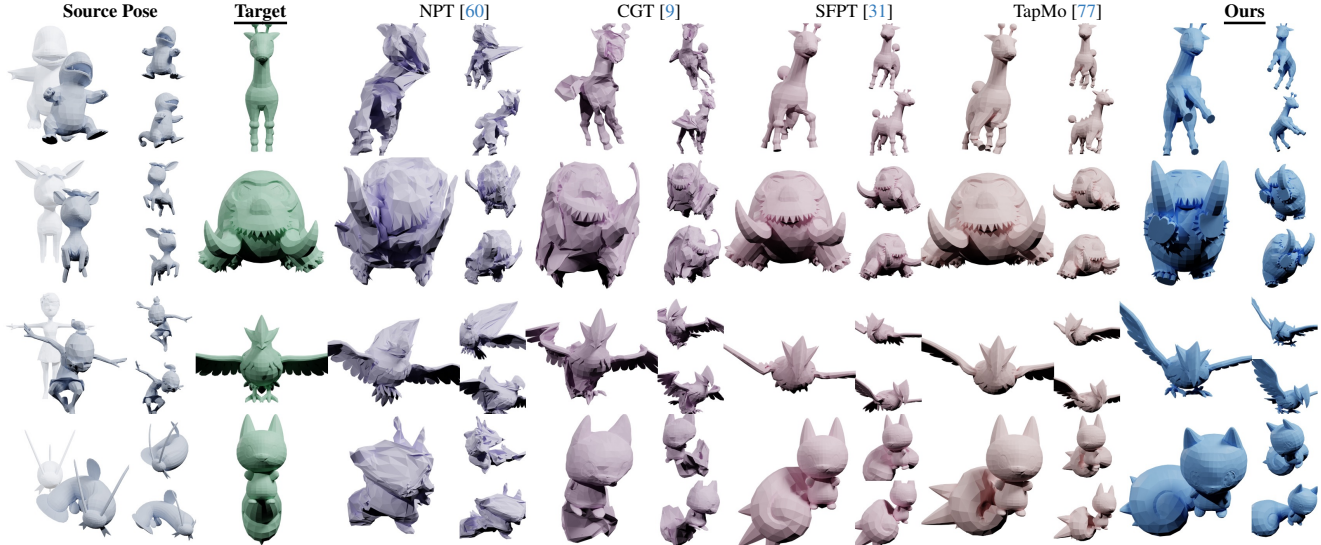


Figure 7. **Qualitative comparisons with existing methods.** We show pose transfer results across a wide range of character categories. From *left to right*: source pose, target character, and results from different methods. Each example is rendered from three viewpoints for comprehensive visual comparisons. Additional qualitative results are provided in the Appendix.

hance mesh smoothness and preserve local geometric details in the final deformed results.

## 4. Experiments

### 4.1. Implementation Details

We implement MimiCAT using PyTorch framework [46] and train it with the AdamW optimizer [34], starting with an initial learning rate of  $1e-4$  for both stages. Our training corpus combines Mixamo [1], AMASS [37], and our newly collected PokeAnimDB, covering diverse and complex shapes and poses. The dataset is split into training, validation, and test sets. In the first stage, we train the correspondence transformer with 384k source-target pairs using a mini-batch size of 128 for 60 epochs. In the second stage, we train the pose transfer transformer for 200 epochs with a mini-batch size of 100, sampling 100k random poses per epoch. All experiments are conducted on 8 NVIDIA A100 GPUs. More details are provided in the Appendix.

### 4.2. Benchmark, Evaluation Metrics & Baselines

**Benchmarks.** We evaluate category-free pose transfer under two settings. (1) *Intra-category transfer*: We select the widely-use Mixamo [1] to assess pose transfer among humanoid characters. Since all Mixamo characters share the same skeleton structure, the ground-truth targets are generated by directly applying the source transformations. We construct 100 character pairs, each with 20 random test poses, resulting in a total of 2,000 evaluation cases. (2) *Cross-category transfer*: To assess generalization beyond specific categories, where ground-truth poses are unavailable, we adopt a cycle-consistency evaluation, where each

method performs pose transfer in both directions, and the consistency between the source and reposed character is measured to quantify transfer quality. We randomly sample 300 character pairs from our dataset and Mixamo, covering both humanoid-to-any and any-to-humanoid settings, with 10 poses per pair, resulting in 3,000 evaluation cases.

**Evaluation Metrics & Baselines.** Following previous works [31, 61, 71], we adopt two metrics for quantitative evaluation: Point-wise Mesh Euclidean Distance (PMD), which measures pose similarity between the predicted and ground-truth deformations, and Edge Length Score (ELS), which evaluates edge consistency after deformation to assess the overall mesh smoothness. We compare MimiCAT against 4 state-of-the-art pose transfer methods [9, 31, 60, 77]. As MimiCAT is among the first to address category-free pose transfer, previous work was originally trained within specific domains. For fair comparison, we re-train or fine-tune their publicly available implementations using the same mixed-character training data described in Sec. 4.1.

### 4.3. Qualitative Comparisons

In Fig. 7, we present qualitative results for category-free pose transfer across diverse character types, including humanoids, fishes, quadrupeds, and birds, demonstrating the robustness of MimiCAT compared to prior methods. Previous approaches (*e.g.*, NPT [60] and CGT [9]) rely on self-supervised learning within paired data of similar characters, limiting their ability to generalize to unseen categories. SFPT [31] and TapMo [77] depend on a fixed number of handle points for deformation, which restricts them to one-to-one mappings and leads to artifacts or twisted poses when transferring across topologically different char-

Table 2. **Quantitative comparisons with existing methods.** We report PMD ( $\times 100$ ) and ELS metrics for humanoid-to-humanoid (H2H) and cross-category transfer (CCT) settings.

Methods	H2H		CCT	
	PMD $\downarrow$	ELS $\uparrow$	PMD $\downarrow$	ELS $\uparrow$
NPT [60]	6.334	0.842	9.889	0.260
CGT [9]	5.687	0.887	6.314	0.744
SFPT [31]	3.616	0.888	4.312	0.913
TapMo [77]	5.078	0.877	4.883	0.922
w/o Eq. 4 (A1)	4.439	0.920	4.524	0.924
w/o Eq. 8 (A2)	4.161	0.920	4.655	0.922
w/o Eq. 5 (A3)	4.268	0.919	4.612	0.922
<b>MimiCAT (Ours)</b>	<b>3.570</b>	<b>0.923</b>	<b>4.264</b>	<b>0.927</b>

acters. In contrast, the proposed MimiCAT leverages soft keypoint correspondences for flexible many-to-many mappings, enabling natural and semantically consistent pose transfer across morphologically diverse characters. For instance, in the *third row*, a human pose with arms fully extended is vividly transferred to a bird spreading its wings, while maintaining structural consistency such as the alignment between the human thighs and bird claws.

#### 4.4. Quantitative Comparisons

Quantitative results are shown in Tab. 2, with the best results **bolded**. NPT [60] and CGT [9] are designed for transferring poses with same topology, therefore their performance degrades noticeably in cross-category scenarios. SFPT [31] and TapMo [77] show improved generalization in category-free scenarios but remain constrained by their one-to-one correspondence assumption. In contrast, MimiCAT consistently achieves the best results across both settings, which demonstrate that our model effectively captures and transfers pose characteristics even across characters with distinct structures and topologies. These gains stem from our shape-aware transformer design, which leverages geometric priors and flexible, length-variant keypoint correspondences to enable robust and accurate pose transfer.

#### 4.5. Application of MimiCAT

The category-free nature of MimiCAT enables it to serve as a plug-and-play module for text-to-any-character motion generation, greatly expanding the applicability of existing T2M systems. As shown in Fig. 8, we take motions produced by off-the-shelf T2M models [14, 23]—originally defined on SMPL skeletons [33, 47]—and use MimiCAT to transfer them frame-by-frame into a wide variety of target characters, yielding diverse and visually compelling animations. This demonstrates the potential of MimiCAT as a general-purpose motion adapter for downstream tasks.

#### 5. Ablation Study

**Settings.** To assess the contribution of each key component in MimiCAT, we conduct ablation studies by removing

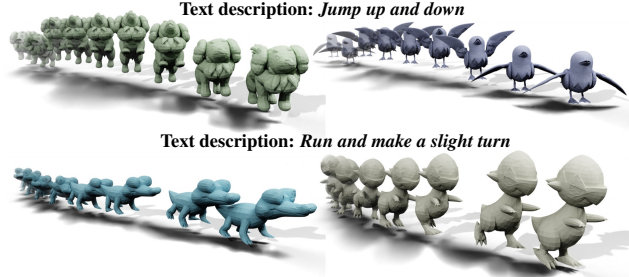


Figure 8. **Application of MimiCAT on motion generation.** We demonstrate that MimiCAT can be zero-shot integrated with standard text-to-motion models [14, 23], allowing generated human motions to be transferred into diverse target characters.

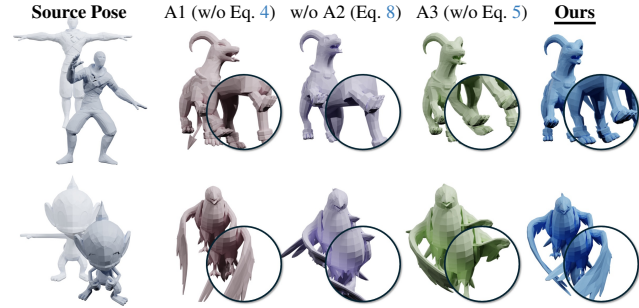


Figure 9. **Ablation studies.** We qualitatively evaluate the impact of key design choices in MimiCAT. From left to right: source pose, and the transferred results produced by each ablated variant. The results show that each component is essential, and removing any of them noticeably degrades the transfer quality.

or replacing individual modules while keeping other parts unchanged for fair comparison. Specifically, we evaluate: **A1** (w/o Eq. 4): replacing our rotation initialization with a simple equal weighted sum instead of the blending scheme in Eq. 4; **A2** (w/o Eq. 8): removing the pose prior regularization; and **A3** (w/o Eq. 5): pretraining the correspondence module  $\mathcal{G}$  using hierarchical correspondence algorithm [66, 74] instead of text-based supervision.

**Results.** The qualitative and quantitative comparisons are shown in Fig. 9 and Tab. 2, respectively. Without the pose prior (A2), unnatural deformations such as joint twisting and self-intersections occur, showing that motion priors learned from large-scale motion datasets help constrain plausible transformations. Using naive rotation averaging (A1) introduces orientation ambiguity, often causing distorted poses (e.g., limbs and wings in target characters). Finally, replacing text-based supervision with heuristic correspondences (A3) leads to misaligned mappings—e.g., a dog’s hind legs being incorrectly matched to the source’s arms—highlighting the necessity of semantic alignment in correspondence learning. Overall, the full MimiCAT achieves the best transfer quality, validating the complementary effects of each component in enabling robust and semantically consistent pose transfer.

## 6. Conclusion

This paper introduces MimiCAT, a cascade-transformer framework supported by a new large-scale motion dataset, PokeAnimDB, to advance 3D pose transfer toward a general, category-free setting. To the best of our knowledge, this is among the first works to enable pose transfer across structurally diverse characters. Benefit from the million-scale pose diversity of PokeAnimDB, MimiCAT learns flexible soft correspondences and shape-aware deformations, enabling plausible transfer across characters with drastically different geometries. We further demonstrate the versatility of MimiCAT in downstream applications such as animation and virtual content creation. We believe PokeAnimDB will serve as a valuable resource for broader vision tasks and inspire future research within the community.

## References

- [1] Mixamo. Online service by Adobe., 2025. Accessed: Jan 2025. [2](#), [3](#), [7](#), [15](#)
- [2] Kfir Aberman, Peizhuo Li, Dani Lischinski, Olga Sorkine-Hornung, Daniel Cohen-Or, and Baoquan Chen. Skeleton-aware networks for deep motion retargeting. *ACM Transactions on Graphics*, 39(4):62, 2020. [3](#)
- [3] Noam Aigerman, Kunal Gupta, Vladimir G Kim, Siddhartha Chaudhuri, Jun Saito, and Thibault Groueix. Neural jacobian fields: learning intrinsic mappings of arbitrary meshes. *ACM Transactions on Graphics*, 41(4):109:1–109:17, 2022. [1](#), [3](#)
- [4] Ilya Baran, Daniel Vlasic, Eitan Grinspun, and Jovan Popović. Semantic deformation transfer. *ACM Transactions on Graphics*, 28(3):36, 2009. [3](#)
- [5] Mirela Ben-Chen, Ofir Weber, and Craig Gotsman. Spatial deformation transfer. In *Proceedings of the 2009 ACM SIGGRAPH/Eurographics Symposium on Computer Animation*, pages 67–74, 2009. [3](#)
- [6] Paul J Besl and Neil D McKay. Method for registration of 3-d shapes. In *Sensor fusion IV: control paradigms and data structures*, pages 586–606. SPIE, 1992. [5](#)
- [7] Sihun Cha, Serin Yoon, Kwanggyoohn Seo, and Junyong Noh. Neural face skinning for mesh-agnostic facial expression cloning. *Computer Graphics Forum*, 44(2), 2025. [3](#)
- [8] Haoyu Chen, Hao Tang, Henglin Shi, Wei Peng, Nicu Sebe, and Guoying Zhao. Intrinsic-extrinsic preserved gans for unsupervised 3d pose transfer. In *Proceedings of the IEEE/CVF International Conference on Computer Vision*, pages 8630–8639, 2021. [1](#), [3](#)
- [9] Haoyu Chen, Hao Tang, Zitong Yu, Nicu Sebe, and Guoying Zhao. Geometry-contrastive transformer for generalized 3d pose transfer. In *Proceedings of the AAAI Conference on Artificial Intelligence*, pages 258–266, 2022. [1](#), [7](#), [8](#), [17](#)
- [10] Haoyu Chen, Hao Tang, Radu Timofte, Luc V Gool, and Guoying Zhao. LART: neural correspondence learning with latent regularization transformer for 3d motion transfer. *Advances in Neural Information Processing Systems*, 36:43742–43753, 2023. [3](#)
- [11] Haoyu Chen, Hao Tang, Ehsan Adeli, and Guoying Zhao. Towards robust 3d pose transfer with adversarial learning. In *Proceedings of the IEEE/CVF Conference on Computer Vision and Pattern Recognition*, pages 2295–2304, 2024. [3](#)
- [12] Jinnan Chen, Chen Li, and Gim Hee Lee. Weakly-supervised 3d pose transfer with keypoints. In *Proceedings of the IEEE/CVF International Conference on Computer Vision*, pages 15156–15165, 2023. [3](#)
- [13] Ling-Hao Chen, Yuhong Zhang, Zixin Yin, Zhiyang Dou, Xin Chen, Jingbo Wang, Taku Komura, and Lei Zhang. Motion2Motion: Cross-topology motion transfer with sparse correspondence. In *SIGGRAPH Asia*, 2025. [3](#)
- [14] Xin Chen, Biao Jiang, Wen Liu, Zilong Huang, Bin Fu, Tao Chen, and Gang Yu. Executing your commands via motion diffusion in latent space. In *Proceedings of the IEEE/CVF conference on Computer Vision and Pattern Recognition*, pages 18000–18010, 2023. [8](#)
- [15] Matt Deitke, Ruoshi Liu, Matthew Wallingford, Huong Ngo, Oscar Michel, Aditya Kusupati, Alan Fan, Christian Laforte, Vikram Voleti, Samir Yitzhak Gadre, et al. Objaverse-XL: A universe of 10m+ 3d objects. *Advances in Neural Information Processing Systems*, 36:35799–35813, 2023. [3](#)
- [16] Yufan Deng, Yuhao Zhang, Chen Geng, Shangzhe Wu, and Jiajun Wu. Anymate: A dataset and baselines for learning 3d object rigging. In *Proceedings of the Special Interest Group on Computer Graphics and Interactive Techniques Conference Conference Papers*, pages 1–10, 2025. [2](#), [3](#), [4](#)
- [17] Keyu Du, Jingyu Hu, Haipeng Li, Hao Xu, Haibing Huang, Chi-Wing Fu, and Shuaicheng Liu. Hierarchical neural semantic representation for 3d semantic correspondence. *arXiv preprint arXiv:2509.17431*, 2025. [2](#)
- [18] Lin Gao, Jie Yang, Yi-Ling Qiao, Yu-Kun Lai, Paul L Rosin, Weiwei Xu, and Shihong Xia. Automatic unpaired shape deformation transfer. *ACM Transactions on Graphics*, 37(6):1–15, 2018. [3](#)
- [19] Igor Gilitschenski, Roshni Sahoo, Wilko Schwarting, Alexander Amini, Sertac Karaman, and Daniela Rus. Deep orientation uncertainty learning based on a bingham loss. In *International Conference on Learning Representations*, 2019. [13](#)
- [20] Michael Gleicher. Retargetting motion to new characters. In *Proceedings of the 25th annual conference on Computer graphics and interactive techniques*, pages 33–42, 1998. [3](#)
- [21] Chuan Guo, Shihao Zou, Xinxin Zuo, Sen Wang, Wei Ji, Xingyu Li, and Li Cheng. Generating diverse and natural 3d human motions from text. In *Proceedings of the IEEE/CVF Conference on Computer Vision and Pattern Recognition*, pages 5152–5161, 2022. [2](#)
- [22] Seokhyeon Hong, Soojin Choi, Chaelin Kim, Sihun Cha, and Junyong Noh. ASMR: Adaptive Skeleton-Mesh Rigging and Skinning via 2D Generative Prior. In *Computer Graphics Forum*. Wiley Online Library, 2025. [3](#)
- [23] Biao Jiang, Xin Chen, Wen Liu, Jingyi Yu, Gang Yu, and Tao Chen. MotionGPT: Human Motion as a Foreign Language. *Advances in Neural Information Processing Systems*, 36:20067–20079, 2023. [8](#)

[24] Ladislav Kavan. Part i: direct skinning methods and deformation primitives. In *SIGGRAPH Course 2014*, pages 1–11, 2014. 3

[25] John T Kent, Asaad M Ganeiber, and Kanti V Mardia. A new method to simulate the bingham and related distributions in directional data analysis with applications. *arXiv preprint arXiv:1310.8110*, 2013. 15

[26] Harold W Kuhn. The hungarian method for the assignment problem. *Naval research logistics quarterly*, 2(1-2):83–97, 1955. 6

[27] Wonkwang Lee, Jongwon Jeong, Taehong Moon, Hyeon-Jong Kim, Jaehyeon Kim, Gunhee Kim, and Byeong-Uk Lee. How to Move Your Dragon: Text-to-Motion Synthesis for Large-Vocabulary Objects. In *International Conference on Machine Learning*, 2025. 1

[28] Peizhuo Li, Kfir Aberman, Rana Hanocka, Libin Liu, Olga Sorkine-Hornung, and Baoquan Chen. Learning skeletal articulations with neural blend shapes. *ACM Transactions on Graphics*, 40(4):130:1–130:15, 2021. 3

[29] Tianyu Li, Jungdam Won, Alexander Clegg, Jeonghwan Kim, Akshara Rai, and Sehoon Ha. ACE: adversarial correspondence embedding for cross morphology motion retargeting from human to nonhuman characters. In *SIGGRAPH Asia 2023 Conference Papers*, pages 46:1–46:11, 2023. 3

[30] Yang Li, Hikari Takehara, Takafumi Taketomi, Bo Zheng, and Matthias Nießner. 4dcomplete: Non-rigid motion estimation beyond the observable surface. In *Proceedings of the IEEE/CVF International Conference on Computer Vision*, pages 12706–12716, 2021. 2, 3

[31] Zhouyingcheng Liao, Jimei Yang, Jun Saito, Gerard Pons-Moll, and Yang Zhou. Skeleton-Free Pose Transfer for Stylized 3D Characters. In *European Conference on Computer Vision*, pages 640–656, 2022. 2, 3, 4, 5, 6, 7, 8, 13, 16, 17

[32] Isabella Liu, Zhan Xu, Wang Yifan, Hao Tan, Zexiang Xu, Xiaolong Wang, Hao Su, and Zifan Shi. RigAnything: Template-Free Autoregressive Rigging for Diverse 3D Assets. *ACM Transactions on Graphics*, 44(4):122:1–122:12, 2025. 2

[33] Matthew Loper, Naureen Mahmood, Javier Romero, Gerard Pons-Moll, and Michael J Black. SMPL: a skinned multi-person linear model. *ACM Transactions on Graphics*, 34(6):248:1–248:16, 2015. 2, 8

[34] Ilya Loshchilov and Frank Hutter. Decoupled weight decay regularization. In *International Conference on Learning Representations*, 2019. 7, 15

[35] Zhongjin Luo, Shengcui Cai, Jinguo Dong, Ruibo Ming, Liangdong Qiu, Xiaohang Zhan, and Xiaoguang Han. RaBit: Parametric Modeling of 3D Biped Cartoon Characters with a Topological-Consistent Dataset. In *Proceedings of the IEEE/CVF Conference on Computer Vision and Pattern Recognition*, pages 12825–12835, 2023. 2

[36] Robin Magnet, Jing Ren, Olga Sorkine-Hornung, and Maks Ovsjanikov. Smooth non-rigid shape matching via effective Dirichlet energy optimization. In *International Conference on 3D Vision*, pages 495–504, 2022. 2

[37] Naureen Mahmood, Nima Ghorbani, Nikolaus F Troje, Gerard Pons-Moll, and Michael J Black. AMASS: Archive of motion capture as surface shapes. In *Proceedings of the IEEE/CVF International Conference on Computer Vision*, pages 5442–5451, 2019. 2, 3, 4, 7

[38] F Landis Markley, Yang Cheng, John L Crassidis, and Yaakov Oshman. Averaging quaternions. *Journal of Guidance, Control, and Dynamics*, 30(4):1193–1197, 2007. 5

[39] Giulia Martinelli, Nicola Garau, Niccoló Bisagno, and Nicola Conci. Skeleton-aware motion retargeting using masked pose modeling. In *European Conference on Computer Vision*, pages 287–303. Springer, 2024. 3

[40] David Mohlin, Josephine Sullivan, and Gérald Bianchi. Probabilistic orientation estimation with matrix fisher distributions. *Advances in Neural Information Processing Systems*, 33:4884–4893, 2020. 2, 4, 6, 13

[41] Albert Mosella-Montoro and Javier Ruiz-Hidalgo. Skinningnet: Two-stream graph convolutional neural network for skinning prediction of synthetic characters. In *Proceedings of the IEEE/CVF Conference on Computer Vision and Pattern Recognition*, pages 18593–18602, 2022. 2

[42] Sanjeev Muralikrishnan, Niladri Shekhar Dutt, and Niloy J Mitra. SMF: Template-free and Rig-free Animation Transfer using Kinetic Codes. *arXiv preprint arXiv:2504.04831*, 2025. 1, 3

[43] Yaakov Oshman and Avishy Carmi. Attitude estimation from vector observations using a genetic-algorithm-embedded quaternion particle filter. *Journal of Guidance, Control, and Dynamics*, 29(4):879–891, 2006. 5

[44] Gautam Pai, Jing Ren, Simone Melzi, Peter Wonka, and Maks Ovsjanikov. Fast sinkhorn filters: Using matrix scaling for non-rigid shape correspondence with functional maps. In *Proceedings of the IEEE/CVF Conference on Computer Vision and Pattern Recognition*, pages 384–393, 2021. 2

[45] Xiaoyu Pan, Jiancong Huang, Jiaming Mai, He Wang, Honglin Li, Tongkui Su, Wenjun Wang, and Xiaogang Jin. Heterskinnet: A heterogeneous network for skin weights prediction. *Proceedings of the ACM on Computer Graphics and Interactive Techniques*, 4(1):1–19, 2021. 2

[46] Adam Paszke, Sam Gross, Francisco Massa, Adam Lerer, James Bradbury, Gregory Chanan, Trevor Killeen, Zeming Lin, Natalia Gimelshein, Luca Antiga, et al. Pytorch: An imperative style, high-performance deep learning library. *Advances in neural information processing systems*, 32, 2019. 7

[47] Georgios Pavlakos, Vasileios Choutas, Nima Ghorbani, Timo Bolkart, Ahmed AA Osman, Dimitrios Tzionas, and Michael J Black. Expressive body capture: 3D hands, face, and body from a single image. In *Proceedings of the IEEE/CVF Conference on Computer Vision and Pattern Recognition*, pages 10975–10985, 2019. 8

[48] Sigal Raab, Inbal Leibovitch, Guy Tevet, Moab Arar, Amit H Bermano, and Daniel Cohen-Or. Single motion diffusion. In *International Conference on Learning Representations*, 2024. 1

[49] Alec Radford, Jong Wook Kim, Chris Hallacy, Aditya Ramesh, Gabriel Goh, Sandhini Agarwal, Girish Sastry, Amanda Askell, Pamela Mishkin, Jack Clark, et al. Learning transferable visual models from natural language super-

vision. In *International Conference on Machine Learning*, pages 8748–8763. PMLR, 2021. 6

[50] Akash Sengupta, Ignas Budvytis, and Roberto Cipolla. Hierarchical kinematic probability distributions for 3D human shape and pose estimation from images in the wild. In *Proceedings of the IEEE/CVF International Conference on Computer Vision*, pages 11219–11229, 2021. 2, 4, 6, 13, 15

[51] Richard Sinkhorn and Paul Knopp. Concerning nonnegative matrices and doubly stochastic matrices. *Pacific Journal of Mathematics*, 21(2):343–348, 1967. 5

[52] Chaoyue Song, Jiacheng Wei, Ruibo Li, Fayao Liu, and Guosheng Lin. 3d pose transfer with correspondence learning and mesh refinement. *Advances in Neural Information Processing Systems*, 34:3108–3120, 2021. 2

[53] Chaoyue Song, Xiu Li, Fan Yang, Zhongcong Xu, Jiacheng Wei, Fayao Liu, Jiashi Feng, Guosheng Lin, and Jianfeng Zhang. Puppeteer: Rig and Animate Your 3D Models. *arXiv preprint arXiv:2508.10898*, 2025. 1, 3

[54] Chaoyue Song, Jianfeng Zhang, Xiu Li, Fan Yang, Yiwen Chen, Zhongcong Xu, Jun Hao Liew, Xiaoyang Guo, Fayao Liu, Jiashi Feng, and Lin Guosheng. MagicArticulate: Make Your 3D Models Articulation-Ready. In *Proceedings of the Computer Vision and Pattern Recognition Conference*, pages 15998–16007, 2025. 2, 3

[55] Olga Sorkine and Marc Alexa. As-rigid-as-possible surface modeling. In *Symposium on Geometry processing*, pages 109–116, 2007. 6

[56] Robert W Sumner and Jovan Popović. Deformation transfer for triangle meshes. *ACM Transactions on graphics*, 23(3):399–405, 2004. 3

[57] Andrea Tagliasacchi, Hao Zhang, and Daniel Cohen-Or. Curve skeleton extraction from incomplete point cloud. In *ACM SIGGRAPH 2009 papers*, pages 1–9. 2009. 2

[58] Truebones Motions Animation Studios. Truebones motion capture library. Online service by Truebones Motions Animation Studios, 2022. Accessed January 2025. 2

[59] Ashish Vaswani, Noam Shazeer, Niki Parmar, Jakob Uszkoreit, Llion Jones, Aidan N Gomez, Łukasz Kaiser, and Illia Polosukhin. Attention is all you need. *Advances in neural information processing systems*, 30, 2017. 2

[60] Jiashun Wang, Chao Wen, Yanwei Fu, Haitao Lin, Tianyun Zou, Xiangyang Xue, and Yinda Zhang. Neural pose transfer by spatially adaptive instance normalization. In *Proceedings of the IEEE/CVF Conference on Computer Vision and Pattern Recognition*, pages 5831–5839, 2020. 1, 2, 3, 7, 8, 17

[61] Jiashun Wang, Xuetong Li, Sifei Liu, Shalini De Mello, Orazio Gallo, Xiaolong Wang, and Jan Kautz. Zero-shot pose transfer for unrigged stylized 3d characters. In *Proceedings of the IEEE/CVF Conference on Computer Vision and Pattern Recognition*, pages 8704–8714, 2023. 1, 2, 7

[62] Runzhong Wang, Junchi Yan, and Xiaokang Yang. Learning combinatorial embedding networks for deep graph matching. In *Proceedings of the IEEE/CVF International Conference on Computer Vision*, pages 3056–3065, 2019. 2, 4

[63] Runzhong Wang, Junchi Yan, and Xiaokang Yang. Combinatorial learning of robust deep graph matching: an embedding based approach. *IEEE transactions on pattern analysis and machine intelligence*, 45(6):6984–7000, 2020. 2, 4

[64] Rong Wang, Wei Mao, Changsheng Lu, and Hongdong Li. Towards high-quality 3d motion transfer with realistic apparel animation. In *European Conference on Computer Vision*, pages 35–51. Springer, 2024. 2, 3

[65] Yuefan Wu, Zeyuan Chen, Shaowei Liu, Zhongzheng Ren, and Shenlong Wang. CASA: Category-agnostic Skeletal Animal Reconstruction. *Advances in Neural Information Processing Systems*, 35:28559–28574, 2022. 2

[66] Pengfei Xu, Yifan Li, Zijin Yang, Weiran Shi, Hongbo Fu, and Hui Huang. Hierarchical layout blending with recursive optimal correspondence. *ACM Transactions on Graphics*, 41(6):249:1–249:15, 2022. 2, 6, 8

[67] Zhan Xu, Yang Zhou, Evangelos Kalogerakis, and Karan Singh. Predicting Animation Skeletons for 3D Articulated Models via Volumetric Nets. In *International Conference on 3D Vision*, pages 298–307, 2019. 2

[68] Zhan Xu, Yang Zhou, Evangelos Kalogerakis, Chris Landreth, and Karan Singh. Rignet: neural rigging for articulated characters. *ACM Transactions on Graphics*, 39(4):58–1, 2020. 2, 3, 4, 6

[69] Wang Yifan, Noam Aigerman, Vladimir G Kim, Siddhartha Chaudhuri, and Olga Sorkine-Hornung. Neural cages for detail-preserving 3d deformations. In *Proceedings of the IEEE/CVF Conference on Computer Vision and Pattern Recognition*, pages 75–83, 2020. 3

[70] Yingda Yin, Yingcheng Cai, He Wang, and Baoquan Chen. Fishermatch: Semi-supervised rotation regression via entropy-based filtering. In *Proceedings of the IEEE/CVF Conference on Computer Vision and Pattern Recognition*, pages 11164–11173, 2022. 2, 4, 13

[71] Seungwoo Yoo, Juil Koo, Kyeongmin Yeo, and Minhyuk Sung. Neural pose representation learning for generating and transferring non-rigid object poses. In *Proceedings of the 38th International Conference on Neural Information Processing Systems*, pages 34349–34377, 2024. 1, 3, 7

[72] Zhenbo Yu, Junjie Wang, Hang Wang, Zhiyuan Zhang, Jinxian Liu, Zefan Li, Bingbing Ni, and Wenjun Zhang. Mesh2animation: Unsupervised animating for quadruped 3d objects. *IEEE Transactions on Circuits and Systems for Video Technology*, 2025. 3

[73] Kwan Yun, Seokhyeon Hong, Chaelin Kim, and Junyoung Noh. Anymole: Any character motion in-betweening leveraging video diffusion models. In *Proceedings of the IEEE/CVF Conference on Computer Vision and Pattern Recognition*, pages 27838–27848, 2025. 1

[74] Xiao Zhan, Rao Fu, and Daniel Ritchie. CharacterMixer: Rig-Aware Interpolation of 3D Characters. *Comput. Graph. Forum*, 43(2):i–iii, 2024. 6, 8

[75] Hao Zhang, Di Chang, Fang Li, Mohammad Soleymani, and Narendra Ahuja. Magicpose4d: Crafting articulated models with appearance and motion control. *Transactions on Machine Learning Research*. 1

[76] Hao Zhang, Haolan Xu, Chun Feng, Varun Jampani, and Narendra Ahuja. PhysRig: Differentiable Physics-Based Skinning and Rigging Framework for Realistic Articulated Object Modeling. *arXiv preprint arXiv:2506.20936*, 2025. 2

[77] Jiaxu Zhang, Shaoli Huang, Zhigang Tu, Xin Chen, Xiaohang Zhan, Gang YU, and Ying Shan. Tapmo: Shape-aware motion generation of skeleton-free characters. In *The Twelfth International Conference on Learning Representations*, 2024. 6, 7, 8, 17

[78] Jia-Peng Zhang, Cheng-Feng Pu, Meng-Hao Guo, Yan-Pei Cao, and Shi-Min Hu. One model to rig them all: Diverse skeleton rigging with unirig. *ACM Transactions on Graphics*, 44(4):123:1–123:18, 2025. 2

[79] Pan Zhang, Bo Zhang, Dong Chen, Lu Yuan, and Fang Wen. Cross-domain correspondence learning for exemplar-based image translation. In *Proceedings of the IEEE/CVF Conference on Computer Vision and Pattern Recognition*, pages 5143–5153, 2020. 2

[80] Qingqing Zhao, Peizhuo Li, Wang Yifan, Sorkine-Hornung Olga, and Gordon Wetzstein. Pose-to-motion: Cross-domain motion retargeting with pose prior. In *Computer Graphics Forum*, page e15170. Wiley Online Library, 2024. 3

[81] Zibo Zhao, Wen Liu, Xin Chen, Xianfang Zeng, Rui Wang, Pei Cheng, Bin Fu, Tao Chen, Gang Yu, and Shenghua Gao. Michelangelo: Conditional 3d shape generation based on shape-image-text aligned latent representation. *Advances in neural information processing systems*, 36:73969–73982, 2023. 2, 3, 5

[82] Keyang Zhou, Bharat Lal Bhatnagar, and Gerard Pons-Moll. Unsupervised shape and pose disentanglement for 3d meshes. In *European Conference on Computer Vision*, pages 341–357. Springer, 2020. 3, 16

# MimiCAT: Mimic with Correspondence-Aware Cascade-Transformer for Category-Free 3D Pose Transfer

## Supplementary Material

This supplementary material provides additional technical details and presents further visualized results supporting the main paper. The content is organized as follows: First, the notations used throughout the paper is summarized in Section A1. Section A2 describes the details of our pose prior model. Section A3 presents further implementation details. Section A4 includes additional qualitative visualizations. Finally, Section A5 discusses the limitations of our method and outlines potential directions for future work.

### A1. Notation Table

For clarity and ease of reference, the key notations used throughout the paper are summarized in Tab. A1.

Table A1. **Summary of important notations.** A consolidated reference of the key variables and symbols used in MimiCAT, grouped according to the modules introduced in the main paper.

Notation	Description
$\bar{\mathbf{V}}^{\text{src}}$	vertices of source character in canonical pose
$\mathbf{V}^{\text{src}}$	vertices of posed source character
$N^{\text{src}}$	number of vertices in source character
$\bar{\mathbf{V}}^{\text{tgt}}$	vertices of target character in canonical pose
$\hat{\mathbf{V}}^{\text{tgt}}$	vertices of posed target character (predicted)
$N^{\text{tgt}}$	number of vertices in target character
$\bar{\mathbf{C}}^{\text{src}}$	canonical keypoints of source character
$\bar{\mathbf{C}}^{\text{tgt}}$	canonical keypoints of target character
$K_1$	number of keypoint of source character
$K_2$	number of keypoint of target character
$f(\mathbf{V}^{\text{A}}, \bar{\mathbf{V}}^{\text{A}}, \bar{\mathbf{V}}^{\text{B}}) \rightarrow \hat{\mathbf{V}}^{\text{B}}$	transferring pose from character A to B
$\mathcal{E}$	pretrained shape encoder
$\mathbf{f}_{\bar{\mathbf{V}}}^{\text{src}}$	shape feature of canonical source character
$\mathbf{f}_{\mathbf{V}}^{\text{src}}$	shape feature of posed source character
$\mathbf{f}_{\bar{\mathbf{V}}}^{\text{tgt}}$	shape feature of canonical target character
$\delta_{\mathbf{f}}$	residual shape feature of source character
$\mathcal{F}$	pose prior transformer
$A(\mathbf{q})$	attitude matrix of quaternion $\mathbf{q}$
$f_M$	shape tokens for $\mathcal{F}$
$f_C$	keypoint tokens for $\mathcal{F}$
$\hat{\mathbf{F}}$	parameters of matrix-Fisher distribution
$c(\mathbf{F}_k)$	distribution normalization constant w.r.t. $\mathbf{F}_k$
$\mathcal{G}$	correspondence transformer
$g_M$	shape tokens for $\mathcal{G}$
$g_C$	keypoint tokens for $\mathcal{G}$
$\mathbf{g}^{\text{src}}$	shape-aware latent representations of source keypoints
$\mathbf{g}^{\text{tgt}}$	shape-aware latent representations of target keypoints
$\mathbf{A}$	learnable weight for affinity matrix of $\mathcal{G}$
$\mathbf{S}$	similarity matrix of source and target keypoints
$\mathbf{f}_k$	CLIP latent feature of keypoint $c_k$
$S_{\text{cos}}$	CLIP-based cosine similarity of keypoint pairs
$\mathbf{M}$	doubly stochastic correspondence matrix
$\mathcal{H}$	pose transfer transformer
$h_M$	shape tokens for $\mathcal{H}$
$h_C$	keypoint tokens for $\mathcal{H}$
$\mathbf{T}^{\text{src}} = \{\mathbf{T}_1^{\text{src}}, \dots, \mathbf{T}_{K_1}^{\text{src}}\}$	per-keypoint transformations for source character
$\mathbf{T}^{\text{tgt}} = \{\hat{\mathbf{T}}_1^{\text{tgt}}, \dots, \hat{\mathbf{T}}_{K_2}^{\text{tgt}}\}$	per-keypoint transformations for target character
$\mathbf{q}_i$	rotation quaternion of $i$ -th keypoint
$\mathbf{t}_i$	translation vector of $i$ -th keypoint

### A2. Details of Pose Prior Transformer

In this section, we provide technical details of the pose prior model, including how we address the challenges arising from varying keypoint lengths and diverse rotation behaviors across characters, as well as the training objectives.

#### A2.1. Architecture of Pose Prior Model

We observe that without proper priors or regularization, the pose transfer model often suffers from severe degeneration such as collapse. However, directly learning unified rotation representations across characters with highly diverse geometries and skeletal structures is non-trivial. To address this, we leverage our motion dataset to train a probabilistic prior model that explicitly captures the likelihood of skeletal structures together with their associated rotations.

Formally, the rotation of each keypoint is represented by a quaternion  $\mathbf{q} \in \mathbb{S}^3$  [31]. One option is to parameterize this distribution using the Bingham distribution [19]. However, the Bingham distribution requires strong constraints on its parameters, which limits model expressiveness [50]. Instead, we follow previous works [40, 50, 70] to map quaternions to attitude matrices  $\mathbf{R} = A(\mathbf{q}) \in \text{SO}(3)$  and model them using the *matrix-Fisher distribution*, which defines a probability density over  $\text{SO}(3)$ :

$$p(\mathbf{R}_k \mid \mathbf{F}_k) = \frac{1}{c(\mathbf{F}_k)} \exp \left( \text{tr}(\mathbf{F}_k^\top \mathbf{R}_k) \right), \quad (\text{A1})$$

where  $\mathbf{F}_k \in \mathbb{R}^{3 \times 3}$  is the distribution parameter of the  $k$ -th keypoint, and  $c(\mathbf{F}_k)$  is the normalization constant.

Similar to the cascade-transformer design of MimiCAT, to capture the joint distribution of rotations across all keypoints of arbitrary characters, we design a transformer-based pose prior model  $\mathcal{F}$ . It estimates  $p(\bar{\mathbf{C}}, \mathbf{C}; \mathbf{f}_{\bar{\mathbf{V}}}, \mathbf{f}_V) = \prod_{k=1}^K p(\mathbf{R}_k \mid \mathbf{F}_k)$ , where  $\bar{\mathbf{C}}$  and  $\mathbf{C}$  denote canonical and posed keypoints, and  $\mathbf{f}_{\bar{\mathbf{V}}}$ ,  $\mathbf{f}_V$  are geometry features extracted from the corresponding meshes.

Specifically, we concatenate  $\mathbf{f}_{\bar{\mathbf{V}}}$  and  $\mathbf{f}_V$  and project them through the shape projector to obtain the shape tokens  $f_M \in \mathbb{R}^{l_{\mathcal{E}} \times d_c}$ . For the keypoints tokens, we concatenate the canonical and posed keypoint coordinates  $\bar{\mathbf{C}}$  and  $\mathbf{C}$ , and map them into a  $d_c$ -dimensional latent representation  $f_C \in \mathbb{R}^{K \times d_c}$  via keypoint encoder. The concatenated tokens  $[f_M, f_C]$  are then fed into transformer blocks, which applies attention mechanism to model interactions among keypoints while conditioning on global geometry. Finally, an MLP decoder maps the latent representations to a set of matrix-Fisher distribution parameters



**Figure A1. Additional pose examples from PokeAnimDB.** PokeAnimDB contains diverse and high-quality character poses covering a wide spectrum of species and morphological structures. From *left* to *right*, we present representative pose samples across characters.

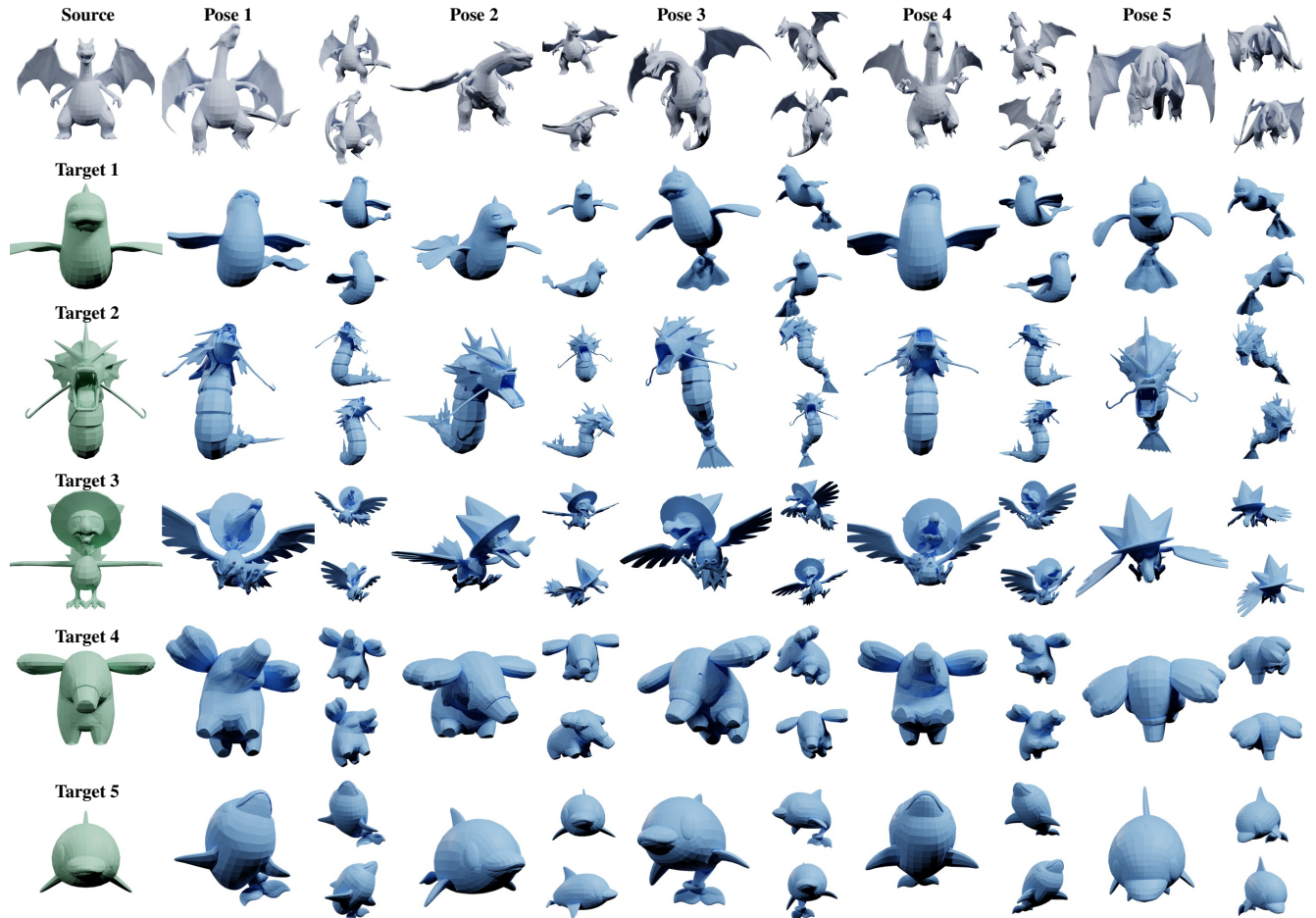


**Figure A2. Qualitative results of MimiCAT (part I).** We present pose transfer results across a wide range of character categories, with each example rendered from three viewpoints. From *left* to *right*: the canonical character followed by its transferred results under five different poses. The *1st* row shows the source character and the five input poses; the *2nd*–*6th* rows show the corresponding transferred poses for each target character.

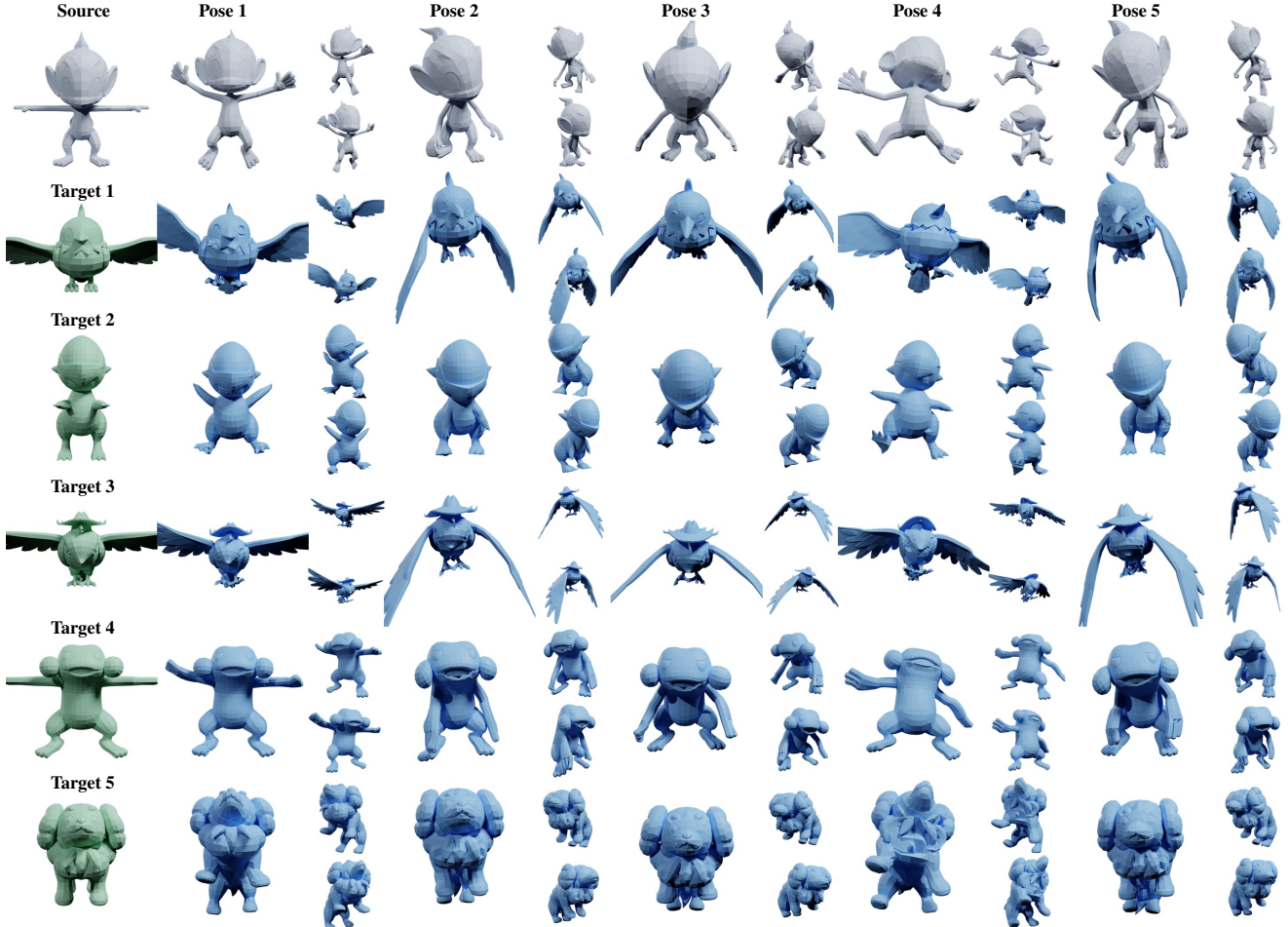


Figure A3. **Qualitative results of MimiCAT (part II).** We present pose transfer results across a wide range of character categories, with each example rendered from three viewpoints. From *left* to *right*: the canonical character followed by its transferred results under five different poses. The *1st* row shows the source character and the five input poses; the *2nd*–*6th* rows show the corresponding transferred poses for each target character.

$\{\hat{\mathbf{F}}_1, \dots, \hat{\mathbf{F}}_K\}$ , where each  $\hat{\mathbf{F}}_k$  models the rotation distribution of the  $k$ -th keypoint.

## A2.2. Training Objective Functions

Following previous works [50],  $\mathcal{F}$  is trained with the negative log-likelihood (NLL) of the ground-truth rotations, with pose sampled from PokeAnimDB and Mixamo [1]:

$$\mathcal{L}_{\text{NLL}} = \sum_{k=1}^K (\log c(\mathbf{F}_k) - \text{tr}(\mathbf{F}_k^\top A(\mathbf{q}_k))). \quad (\text{A2})$$

Additionally, we adopt differentiable rejection sampling [25] to draw  $n$  candidate rotations from the predicted distributions. Combined with the estimated translation vectors, the sampled characters  $\hat{\mathbf{V}}$  are reconstructed via linear blend skinning and supervised against the ground-truth  $\mathbf{V}$  using a reconstruction loss:

$$\mathcal{L}_{\text{sample}} = \frac{1}{n} \sum_{i=1}^n \|\hat{\mathbf{V}}^{(i)} - \mathbf{V}\|_2^2, \quad \mathbf{q}_k^{(i)} \sim p(A(\mathbf{q}_k) | \mathbf{F}_k). \quad (\text{A3})$$

The pose prior transformer is trained using AdamW [34] with an initial learning rate of  $1e-4$ , a mini-batch size of 256, for a total of 5 epochs. As such, once the probability model is trained, it predicts the distribution parameters for a given canonical-posed keypoint pair. During pose transfer, we regularize the predicted rotations by maximizing their likelihood under these learned distributions, ensuring that the estimated joint rotations remain plausible for the given character geometry.

## A3. Implementation Details

### A3.1. Model Details of MimiCAT

For all modules—the pose prior transformer  $\mathcal{F}$ , the correspondence transformer  $\mathcal{G}$ , and the pose transfer transformer  $\mathcal{H}$ —we adopt a similar architectural design. The keypoint encoder and shape projector first map their respective inputs into 256-dimensional latent tokens, keypoint encoder is implemented with a 2-layer MLP and shape projector is

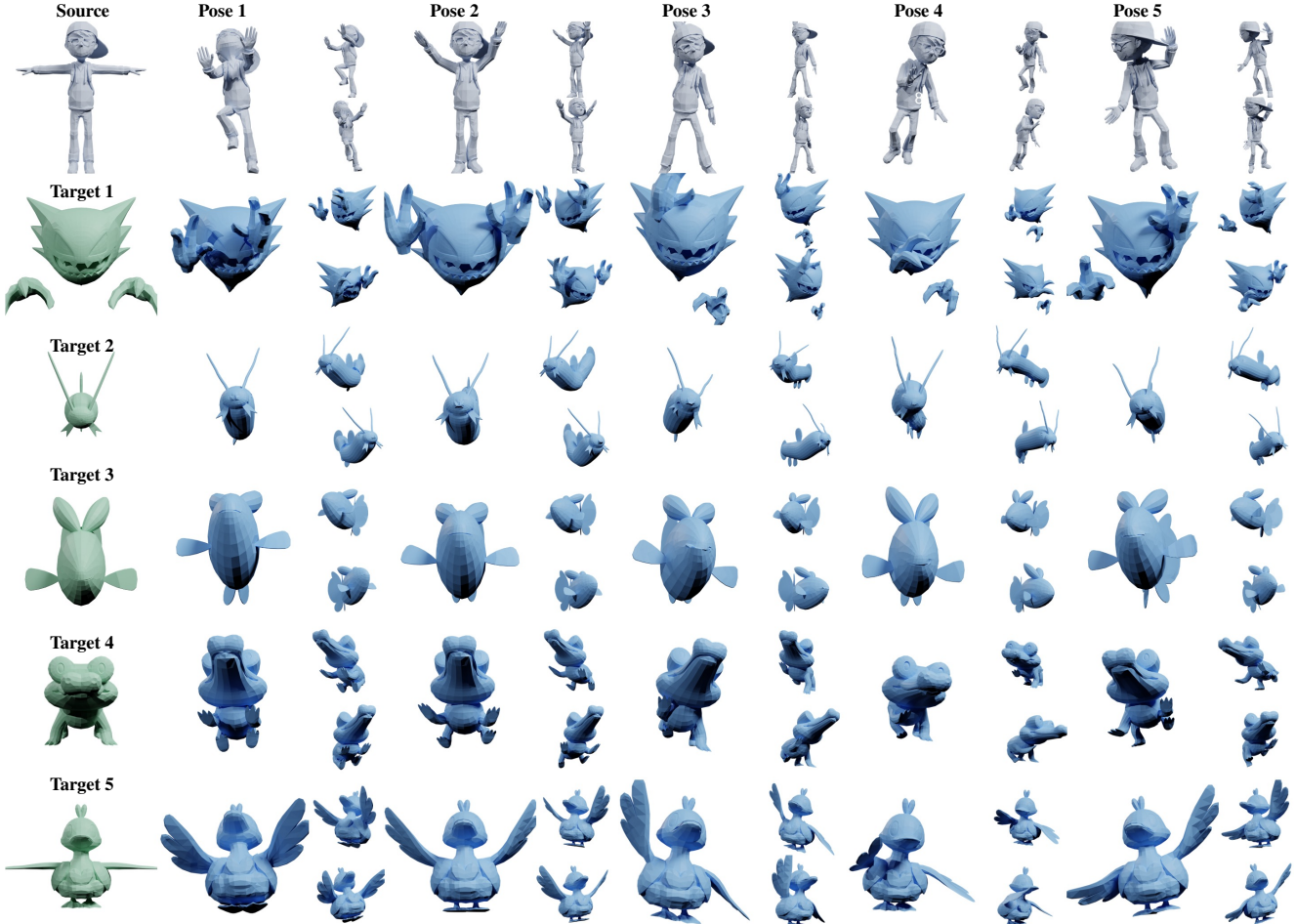


Figure A4. **Qualitative results of MimiCAT (part III).** We present pose transfer results across a wide range of character categories, with each example rendered from three viewpoints. From *left* to *right*: the canonical character followed by its transferred results under five different poses. The *1st* row shows the source character and the five input poses; the *2nd*–*6th* rows show the corresponding transferred poses for each target character.

a linear layer, with hidden dimension of 1,024.

For  $\mathcal{F}$ ,  $\mathcal{G}$ , and  $\mathcal{H}$ , each module adopts a 6-layer stacked transformer encoder, where every layer comprises a multi-head self-attention (MHSA) module (with 8 heads) followed by a 2-layer MLP. The MLP uses a hidden dimension of 2,048. The distribution decoder of  $\mathcal{F}$  is a 2-layer MLP with a hidden dimension of 128 and nonlinear activation. For the correspondence module  $\mathcal{G}$ , the learnable weights  $\mathbf{A}$  is parameterized with a hidden dimension of 256. The transformation decoder of  $\mathcal{H}$  is implemented as an MLP with a hidden dimension of 256.

### A3.2. Details of Dataset Split

For the AMASS dataset, we follow the standard protocol in prior works [31, 82] and split the motions into training and validation sets. For Mixamo, we use 97 characters for training and 11 for testing. For PokeAnimDB, we split the dataset into 780 training characters, 109 validation characters, and 86 test characters. Across these sources, we use

a total of 4.21 million pose samples to train the pose prior transformer  $\mathcal{F}$ . For the correspondence transformer  $\mathcal{G}$ , we construct 384k canonical-pose pairs for training. To train the pose transfer transformer  $\mathcal{H}$ , we sample 100k source-target character pairs from the training split at each epoch, drawing random pose for each pair during every iteration.

## A4. Additional Visualized Results

### A4.1. Details of PokeAnimDB

As stated in the main paper, PokeAnimDB provides character-level motion sequences, forming a large-scale corpus of diverse 3D character poses. Each character is associated with a set of predefined motion clips spanning various action categories. On average, a character contains approximately 30 actions, with the number ranging from 3 to 102. Fig. A1 further illustrates the diversity of poses and character types captured in our dataset.

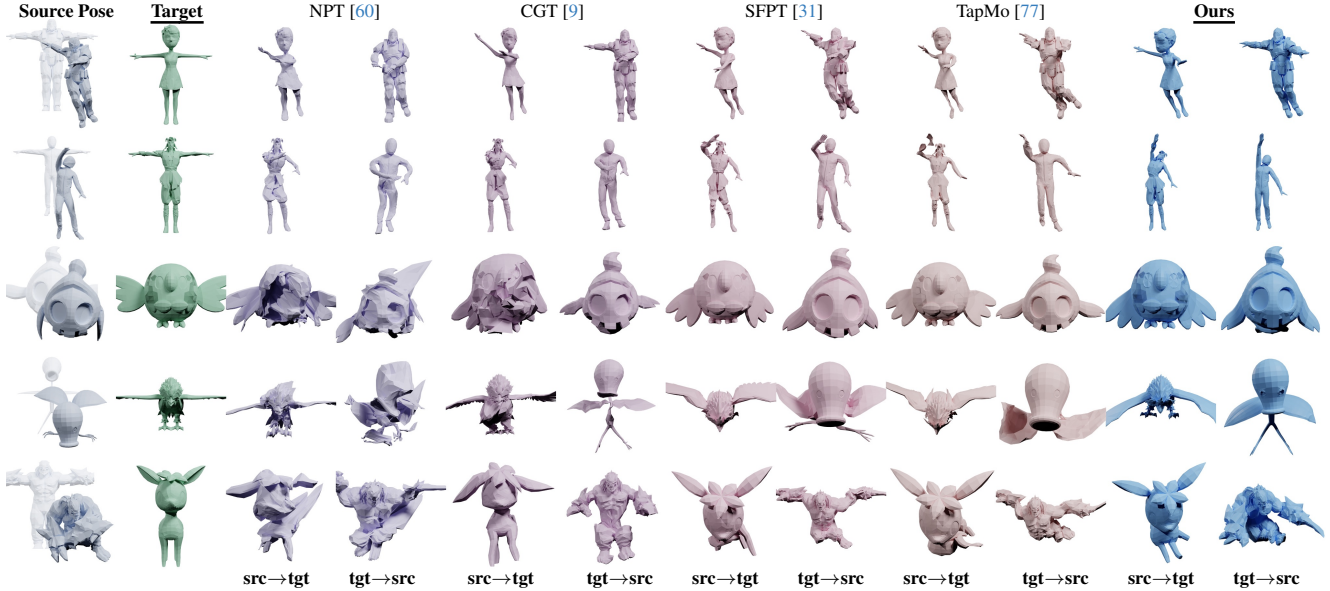


Figure A5. **Qualitative cycle-consistency comparisons with existing methods.** From *left* to *right*: source character, target character, and bidirectional pose transfer results (source→target and target→source) produced by different methods. MimiCAT consistently yields higher-quality transfers with more realistic poses and fewer distortions.

#### A4.2. Visualized Results from MimiCAT

In Fig. A2, A3, and A4, we present additional qualitative pose transfer results produced by MimiCAT. For each source character, we transfer 5 distinct poses to 5 target characters spanning diverse categories. The results further demonstrate that MimiCAT can reliably transfer poses across structurally different characters, faithfully preserving geometric details while capturing the pose characteristics from the source characters.

#### A4.3. Cycle Consistency Comparison

As a supplement to our quantitative evaluation, we provide additional visual comparisons of pose transfer quality in Fig. A5. For each method, we show both the transferred target poses and the corresponding cycled-source reconstructions. The first two rows show examples of humanoid-to-humanoid transfer, where we also include cycle-consistency results for reference. The remaining three rows illustrate a variety of cross-category transfer cases, covering challenging scenarios with large geometric and topological discrepancies. These visualizations qualitatively confirm our quantitative findings: MimiCAT achieves the smallest PMD while preserving mesh smoothness (highest ELS), producing more plausible transfer results than prior baselines.

### A5. Limitation & Future Work

Although MimiCAT achieves state-of-the-art performance compared to existing baselines, it still has several limitations. In this section, we discuss the limitations of our work and outline several future research directions.

First, our framework relies on keypoints and skin weights predicted by pretrained models. Errors in this stage may propagate to the downstream pose transfer pipeline and negatively affect the final results. In the future, we plan to explore an optimization framework that jointly updates the skin weights, keypoints, and target transformations, such that they coherently contribute to the final transfer quality.

Second, as the exploration of efficient transformer architectures is beyond the scope of this work, MimiCAT adopts computationally expensive vanilla attention implementations. An important extension would be to incorporate more efficient attention mechanisms (e.g., linear or sparse attention) to reduce computational cost while maintaining—or potentially improving—the quality of pose transfer.

Finally, while we demonstrate that MimiCAT can serve as a plug-and-play module for zero-shot text-to-any-character motion generation, the current pipeline does not explicitly enforce temporal consistency across frames. Incorporating temporal modeling could significantly improve motion-level coherence and stability. In future work, we plan to leverage the dataset introduced in this paper to further advance 4D generation and general motion synthesis.